Environmental and Experimental Botany 188 (2021) 104515

Contents lists available at ScienceDirect

Environmental and Experimental Botany

journal homepage: www.elsevier.com/locate/envexpbot

Metabolic coordination of rice seed development to nighttime warming: In-situ determination of cellular redox states using picolitre pressure-probe electrospray-ionization mass spectrometry

Fang-Yu Chang [a,b], Yuto Hatakeyma [c,d], Hiroshi Nonami [d], Rosa Erra-Balsells [e], Takuya Araki [a,d], Hiroshi Nakano [c], Hiroshi Wada [a,c,d,*]

[a] The United Graduate School of Agricultural Sciences, Ehime University, Matsuyama, Ehime, Japan
[b] Kaohsiung District Agricultural Research and Extension Station, Council of Agriculture, Executive Yuan, Pingtung, Taiwan
[c] Kyushu Okinawa Agricultural Research Center, National Agriculture and Food Research Organization, Chikugo, Fukuoka, Japan
[d] Graduate School of Agriculture, Ehime University, Matsuyama, Ehime, Japan
[e] Department of Organic Chemistry and CIHIDECAR (CONICET), University of Buenos Aires, Buenos Aires, Argentina

ARTICLE INFO

Keywords:
Ascorbic acid
Chalkiness
Embryo development
Glutathione
High night temperature
Oryza sativa
Redox
Single-cell analysis

ABSTRACT

High night temperature (HNT) at the ripening stage severely affects both rice yield and quality. HNT accelerates embryo growth and chalky formation in the developing grains, accompanying with a diminishment of endosperm cell size. Although these responses may be physiologically interacted each other in the grains, what signals are involved in the accelerated embryo development remains undetermined. In this work, we have used picolitre pressure-probe electrospray-ionization mass spectrometry (picoPPESI-MS) to conduct single-cell metabolomics at several regions in HNT-treated grains, embryonic scutellum and outer endosperms in the basal ('chalky region' at maturation) and middle ('translucent region' at maturation as a reference) positions. Microscopic observations showed that HNT promoted cell expansion rate in the scutellum. When embryonic cell expansion rate reached the maximum, spatial differences in several metabolisms including ascorbate-glutathione (ASC-GSH) pathway and purine were detected, together with considerable sugar and amino acid accumulations in embryonic scutellum cells. There was no treatment difference in GSH content during active cell expansion in HNT-treated embryos, although an increase in GSH/GSSG ratio due to a reduction in oxidized glutathione (GSSG) content has been contrastingly observed. In the endosperms, greater ASC accumulation with a difference in ASC/dehydroascobic acid ratio has been also detected under HNT conditions. Since dormancy is often correlated with GSSG concentration, it is concluded that spatial regulation of GSH redox homeostasis detected at cell-level might be essential for dormancy alleviation and embryo growth accelerated in HNT-treated seeds.

1. Introduction

Extreme heat-related damages have been widely affecting crop production under ongoing global warming (IPCC, 2013), and it seems likely that this situation has not changed by the temporal economic stagnation during the coronavirus pandemic (WMO, 2020). As the frequency of warmer nighttime is expected to increase in addition to the frequent appearance of heat spikes (IPCC, 2013), an increasing risk of high night temperature (HNT) during the ripening stage is considered to be a major concern in rice production (Peng et al., 2004; Morita et al., 2005; Xu et al., 2020) as well as high day temperature (HDT) from heading to 20 days after heading (DAH) (Jagadish et al., 2015; Morita et al., 2016; Wu et al., 2016). And therefore, further acceleration of heat tolerance incorporating multiple approaches has been strongly desired (Wada, 2019; Xu et al., 2020).

Warmer nights often induce a diminishment of endosperm cell size (Morita et al., 2005; Wada et al., 2021) and a disruption of rice appearance (Morita et al., 2004), resulting in a decline in grain weight (Peng et al., 2004; Morita et al., 2005, 2016; Shi et al., 2017; Wada et al., 2021). Under HNT conditions, growing kernels often accelerate embryo growth, simultaneously turning to chalk in outer endosperms along the basal side and dorsal vasculatures, resulting in the occurrence of basal-white rice and white-back rice (Wada et al., 2021), also observed in HDT conditions (Wada et al., 2019). Because these events occur in the

* Corresponding author. Present address: Graduate School of Agriculture, Ehime University, 3-5-7 Tarumi, Matsuyama, Ehime, 790-8566, Japan.
E-mail address: hwada@agr.ehime-u.ac.jp (H. Wada).

https://doi.org/10.1016/j.envexpbot.2021.104515
Received 24 February 2021; Received in revised form 6 May 2021; Accepted 9 May 2021
Available online 11 May 2021

same grains at HNT/HDT, spatially coordinated certain signal(s) might be involved in dormancy modified under HNT/HDT conditions. However, what increases embryo growth rate in developing seeds under HNT/HDT conditions remains unknown.

Ascorbic acid (ASC) and reduced glutathione (GSH) both play important roles as major scavengers of reactive oxygen species (ROS) (Noctor and Foyer, 1998; Noctor et al., 2002; Maughan and Foyer, 2006; Noctor et al., 2012; Akram et al., 2017). It has been accepted that a certain level of ROS and protein oxidation are required for dormancy breaking (Oracz et al., 2007; El-Maarouf-Bouteau et al., 2013; Bailly, 2019). More recently, Bailly has proposed in dry seeds that spatiotemporal regulation of ROS production cross-talking with hormone signaling controls the cellular events involved in cell expansion during germination (Bailly, 2019). Heat conditions during ripening are known to reduce abscisic acid (ABA) content, causing pre-harvest sprouting in oil rape seeds (Brunel-Muguet et al., 2015). In rice, heat conditions enhanced H_2O_2 production and expression of genes in related to gibberellic acid (GA) biosynthesis and ABA catabolism (Suriyasak et al., 2017). Besides the regulation of ABA and GA on dormancy and germination, an increase in GSH and reduction of GSSG was found in both embryo and endosperm during seed germination (Tommasi et al., 2001). If similar mechanism(s) exists in the developing rice seeds in HNT treatment, there might be spatial treatment differences in redox state closely associated with the regulation of embryo growth.

Cellular redox states are often expressed as the ratios of oxidized/reduced glutathione (GSH/GSSG) and ASC/dehydroascorbic acid (DHA), which have been used as reliable biomarkers of the redox balance in the cells (e.g., Asensi et al., 1999 for GSH/GSSG ratio). Regarding the determination of redox states, the former GSH/GSSG ratio has been determined by mainly using either a fluorescence spectrophotometer or LC-ES/MS at tissue level (e.g., pollen grains, Garcia--Quiros et al., 2020). In analytical chemistry, direct measurement of these redox states in the live single cells, simultaneously characterizing the cellular composition has been a challenging subject. In this work, single-cell metabolomics, picolitre Pressure-Probe Electro-Spray-Ionization Mass Spectrometry (picoPPESI-MS) has been utilized to examine our hypothesis, providing intact 'Koshihikari' rice plants that is susceptible to heat with strong tolerance to pre-harvest sprouting (Kobayashi et al., 2018). We have characterized metabolic changes by collecting the cellular fluids from three types of single cells, located at embryonic scutellum and two endosperm regions in the same kernels developing under nighttime warming. HNT-related changes in cellular metabolisms including GSH and ASC redox states detected at each position will be discussed in terms of embryo development in the seeds.

2. Materials and methods

2.1. Plant materials

A growth-chamber experiment was conducted in Kyushu Okinawa Agricultural Research Center, National Agriculture and Food Research Organization, Chikugo, Japan in 2018, according to the previous work (Wada et al., 2021). The experiment was laid out in a completely randomized design with two treatments (HNT and control) and at least three biological replications for a total of 24 experimental pots. Simply, two-weeks-old *Oryza sativa* L. 'Koshihikari' seedlings were transplanted into plastic pots (3.82 L, diameter 0.16 m, and height 0.2 m) containing a lowland paddy soil (Typic Endoaquepts) with a basal dressing of 3.5 g pot^{-1} [commercial fertilizer, 20-10-12 (N-P_2O_5-K_2O)]. Plants were grown by removing the tillers periodically to restrict to its main culm and cultivated in a cycle of day/night air temperatures of 28 °C (13 h, 5:50−18:50)/22 °C (11 h, 18:50−5:50) at 70 %/80 % relative humidity (RH) and 750 μmol photons m^{-2} s^{-1} photosynthetically active radiation set at the plant canopy until heading. Two treatments were applied at the 5th day after heading: no heat as control (28/22 °C and RH 70 %/80 %) and HNT (28/34 °C RH 70 %/80 % with the same light conditions) for 10 days. At 15 DAH, plants treated under HNT conditions were transferred to control chamber to grow until the mature stage (40 DAH).

2.2. Determination of in situ cell metabolites

Single-cell metabolomics using picoPPESI-MS (Nakashima et al., 2016) was carried out at daytime (between 1100 h and 1600 h) in the outer endosperm cells of 1) middle and 2) basal positions and 3) the cells located at the basal part of embryonic scutellum in superior kernels, attached to the primary and secondary pedicels on the first to third primary rachis branches, counted from the top of the panicle. The spikelet kernels were collected at 11 DAH (i.e., approximately 10 days after pollination), whose cell division almost finished and embryo growth rate reached to the maximum (Hoshikawa, 1989), corresponding to the Stage 'Em8' (Itoh et al., 2005), and the hull in the spikelet was removed gently under humid conditions. The kernel was gently fixed on the sample holder using tape. The tip of quartz microcapillary was inserted into the above-mentioned three target cells, developing embryo (referred to as 'EMB') cells (specifically, embryonic scutellum cells) located at approximately 50 μm below epidermis, two outer endosperm (OE) cells (both located between 150−200 μm below nucellar-epidermis) at the basal (referred to as 'BOE', which turns to chalk at maturation) and middle outer endosperms (referred to as 'MOE', which turns to translucent at maturation) in the kernels developing in HNT treatment. For outer endosperms, a 1 mm diameter biopsy punch was used to remove 0.031 cm^2 of pericarp tissue in the basal and lateral side of the kernel prior to the tip insertion to reduce the risk of contamination from each pericarp tissue. At each location, cell sap was collected, and immediately the probe tip was oriented toward the orifice of an Orbitrap mass spectrometer (Q-Exactive, Thermo Fisher Scientific Inc., MA, the US) and was electrified with −4 kV using a high voltage generator (AKTB-05k1PN/S, Touwa Keisoku Corp., Tokyo, Japan) (Nakashima et al., 2016). Using the same instrumental settings described previously (Wada et al., 2021), the negative ion mode MS scan was performed with the instrumental settings of 200 ms as maximum injection time, inlet ion transfer tube temperature of 250 °C, and resolution of 35,000. The intensity threshold was set to be 1000 in this study. All the signals with less than the threshold had been rejected prior to the analysis. When successful impalement and cell sap collection was ensured without tip plugging in each target cell, the entire process of picoPPESI-MS analysis on the cells after the tip impalement was completed within a few minutes. All manipulations were carried out under the digital microscope (KH-8700, HIROX Co. Ltd., Tokyo, Japan), and kernels attached to the sample holder was humidified during all processes. Reported mass spectra at each location are representative of the same experiments with 3–11 independent kernels from at least 3 individual plants in each treatment.

2.3. Identification of cell metabolites

The list of monoisotopic exact m/z values for all the peaks on acquired mass spectra were extracted using "Qual Browser" application in the Thermo Xcalibur software (Thermo Fisher Scientific Inc., MA, USA). According to the previous work (Nakashima et al., 2016), metabolites were identified at less than 5 ppm differences from the theoretical mass-to-charge ratio (m/z) of candidate metabolites in an on-line metabolomics database, Metlin (http://metlin.scripps.edu/index.php).

2.4. Microscopy

Microscopic observation was conducted according to the previous works (Saito et al., 2010) with a slight modification (Hatakeyama et al., 2018). Transverse segments (1−2 mm thick) from the middle of the kernel at 9, 15, and 35 DAH were fixed with 4 % (w/v) paraformaldehyde in 100 mM sodium phosphate (pH 7.2) for 3 h at room temperature and then washed in 100 mM phosphate buffer (pH 7.2).

Fixed tissues were dehydrated through ethanol series, and embedded in LR White resin in the 'hard' formulation (London Resin, Hampshire, UK) by two-days polymerizing at 60 °C. Semi-thin sections (appropriately 900 nm) for light microscopy were stained with 0.1 % (w/v) Coomassie Brilliant Blue for 1 h followed by potassium iodide for 1 min. Sections were cut with an ultramicrotome (Sorvall MT-5000, DuPont, Newtown, CT, USA) using a diamond knife. In some cases, frozen kernels were cut in half and the developing embryos were photographed. For image analysis at 9, 15, and 35 DAH, the light microscopic images taken from three plants, and embryo area (6–10 kernels) and embryonic scutellum cells (84–180 cells from three kernels), where picoPPESI-MS analysis was conducted, were traced by using ImageJ software (National Institutes of Health, Bethesda, MD, USA). For the organelle arrangement image analysis in basal outer endosperm cells at 9, 15, and 35 DAH, the outline of all amyloplasts, protein bodies (PBs), other area (referred to as 'gap') in the cells, as well as the cells on the light microscopic images taken from 16 to 34 cells in three kernels from three plants were traced by using ImageJ software (National Institutes of Health, Bethesda, MD, USA), according to the previous work (Hatakeyama et al., 2018). And, the spatial ratio of each organelle per cell was estimated.

2.5. Kernel quality and weight

Superior kernels attached to the same position of a panicle in each treatment were sampled. The >1.8 mm thickness of dehulled grains were sieved, and their appearance (the numbers of perfect rice (PR), basal-white rice (BWR) and white-back rice (WBR), and other kernels) was visually evaluated with 4 biological replicates (4 panicles) in each treatment, according to the standard evaluation method of The Ministry of Agriculture, Forestry and Fisheries of Japan (https://www.maff.go.jp/j/seisan/syoryu/kensa/kome/k_kikaku/k_kaisetsu/index.html). The dry weight of kernel samples in each treatment with 5–6 biological replicates was determined at harvest, as described previously (Wada et al., 2011). Reported kernel weight values represent averages of 40–48 kernels, respectively, collected from 5 to 6 independent plants.

2.6. Statistical analysis

Significant differences between means were determined using either a *t*-test or a Tukey-Kramer's test in Microsoft Excel and SigmaPlot software (version 14.0, Systat Software Inc.).

3. Results

3.1. Rice appearance quality decreased under HNT conditions

Comparing to control, the appearance of brown rice turned less translucent under HNT treatment (Fig. 1A). The rice appearance in control was composed of 96.3 % PR, 1.1 % BWR and WBR, and 2.6 % other kernels, while the data show that chalky rice composed of BWR

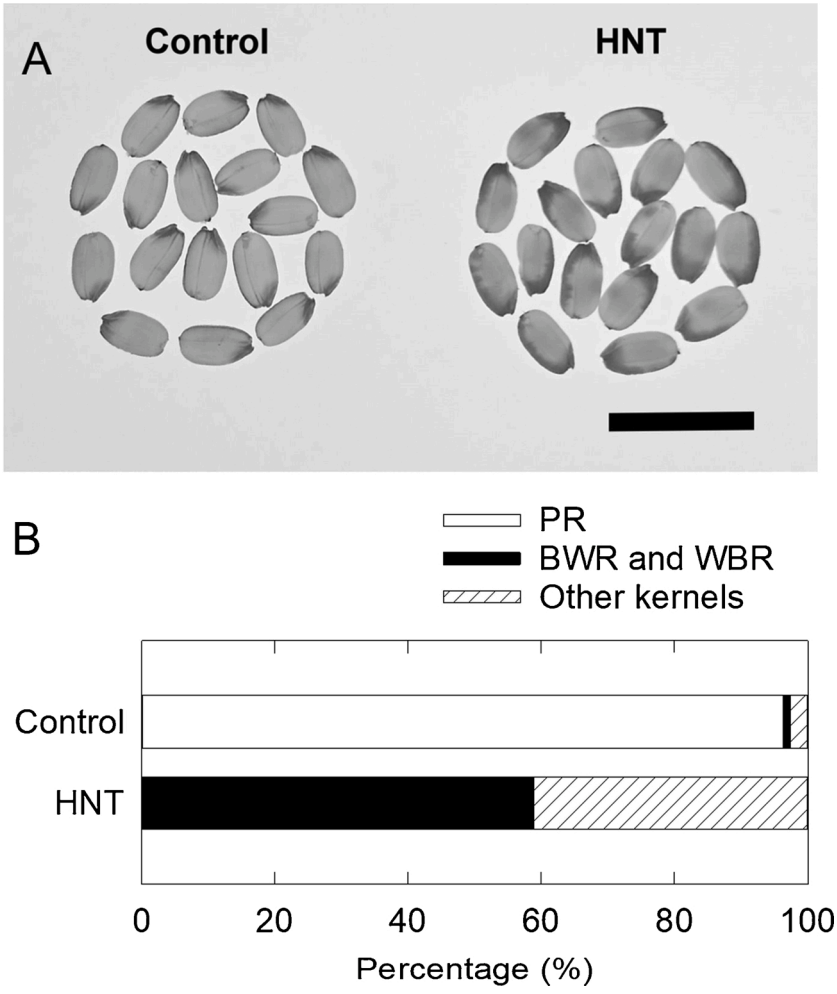

Fig. 1. Images of mature rice grains in control and HNT treatment (A). Percentages of perfect rice (PR), basal-white rice (BWR) with/without white-back rice (WBR), and other kernels (B). Significance at the 0.001, 0.05 and 0.05 probability level between treatments was observed in PR, BWR plus WBR, and other kernels, respectively. Scale bar is 1 cm in (A).

and WBR, and other kernels increased in HNT treatment, reaching to 58.9 % and 41.1 %, respectively, resulting in a considerable decline in PR (0 % under HNT treatment) (Fig. 1B). Kernels with basal-white or white-back symptom(s) but less than the threshold (see Methods) were classified as other kernels (Fig. 1B).

3.2. Microscopic observation under HNT conditions

Dry weight of HNT-treated embryos was higher than that of control (Fig. 2A), whereas dry weight of the rest parts (i.e., endosperm plus aleurone layers and pericarp except for the embryo) was smaller in HNT treatment than in control (Fig. 2B) at maturation. As the results, the ratio of embryo dry weight to entire kernel dry weight became larger in HNT than in control (Fig. 2C). The data show that embryo development was enhanced by HNT between 9 and 15 DAH (Fig. 2A and D–K). The observed HNT-enhanced embryo development was concomitant with an increase in cell size (i.e., cell expansion) (Fig. 2J and K and Table S1), exhibiting with a linear regression between embryo area and embryonic scutellum cell area (inset in Fig. 2K). Based on the observations, picoPPESI-MS analysis described below was conducted at 11 DAH (see the arrows in Fig. 2J and K). CBB and I_2-KI stains were used to identify the distribution of proteins and amyloplasts in each target zone during seed development, respectively. Scutellum and epiblast located at the outer tissues of embryos were less stained by CBB (i.e., light blue), suggesting that embryo cells contain less amount of amyloplasts and protein bodies in HNT treatment than in control (Fig. S1A–F). The close inspection in the embryonic scutellum cells shows that cell division actively occurred at 9 DAH with no clear treatment difference in cell morphology (Fig. S1A and D). Until the relative cell expansion rate declined at 15 DAH (Fig. 2K), numerous organelles including amyloplasts, presumably lipid bodies and protein bodies accumulated in the cells, although the size of amyloplasts was smaller in HNT than control.

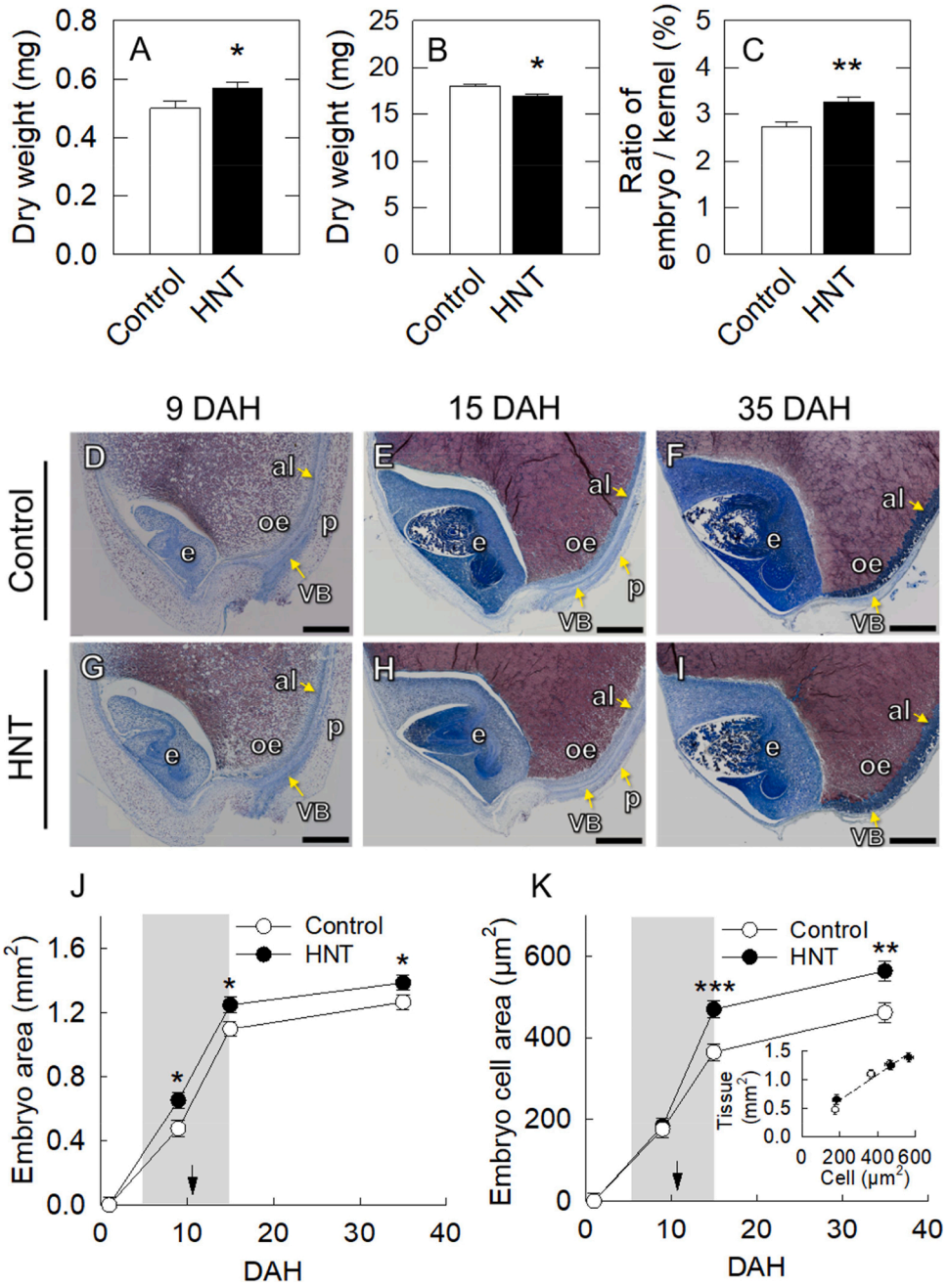

Fig. 2. Dry weight of embryo (A) and the rest of kernel tissue (i.e., endosperm plus aleurone layers and pericarp except for embryo) (B). The ratio of embryo dry weight to dry weight of mature rice kernels (C). Light microscopic images taken at the basal part of kernel sections at 9, 15, and 35 DAH in control (D-F) and high night temperature treatment (G-I). These sections were stained with Coomassie Brilliant Blue and iodine-potassium iodide. al, aleurone layer; e, embryo; oe, outer endosperm; p, pericarp; VB, vascular bundle. Time course of changes in area of embryos (J) and embryonic scutellum cells (K), where picoPPESI-MS analysis was conducted (see Fig. 3). The inserted graph in (K) shows the relation of embryo tissue and embryo cell; the dashed line indicates a linear regression line ($r^2 = 0.958$, $p < 0.001$). The gray area in (J and K) indicates the duration of HNT treatment. The arrow indicates 11 DAH, at which picoPPESI-MS was performed. Data in (A-C) are the mean ± SE of 40-48 superior kernels from 5-6 individual plants. Data in (J) are the mean ± SE of 6-10 superior kernels from 3 individual plants. Data in (K) are the mean ± SE of 84-180 individual cells collected from 3 plants. *, ** and *** show $p <$ 0.05, 0.01 and 0.001 by *t*- test, respectively. Scale bars are 400 μm in (D–I).

Some vacuoles were also observed in HNT-treated cells, but little for control (Fig. S1B and E). In the cells at 35 DAH, large size of amyloplasts were observed in control, whereas the relatively small size of amyloplasts together with presumably lipid bodies, numerous small vacuoles, and PBs remained in the cytosol in the HNT-treated cells (Fig. S1C and F). In addition, aleurone layers in HNT treatment became thicker than control towards 35DAH (Fig. S1G-L). Time course of changes in major organelle components located at BOE (Fig. S2) showed that percentage of amyloplasts and protein bodies increased in accordance with a decrease in gap area during normal grain development (Fig. S2A–C). After 15 DAH, the percentage of gap area in HNT treatment was larger than control, whereas the percentage of both amyloplasts and protein bodies in HNT treatment were lower than in control (Fig. S2G–I). Higher percentage of gap area composed of vacuolar compartments was observed in HNT treated BOE cells at 35 DAH (Fig. S2F and I), resulting in air space formation to turn chalk (Fig. 1A).

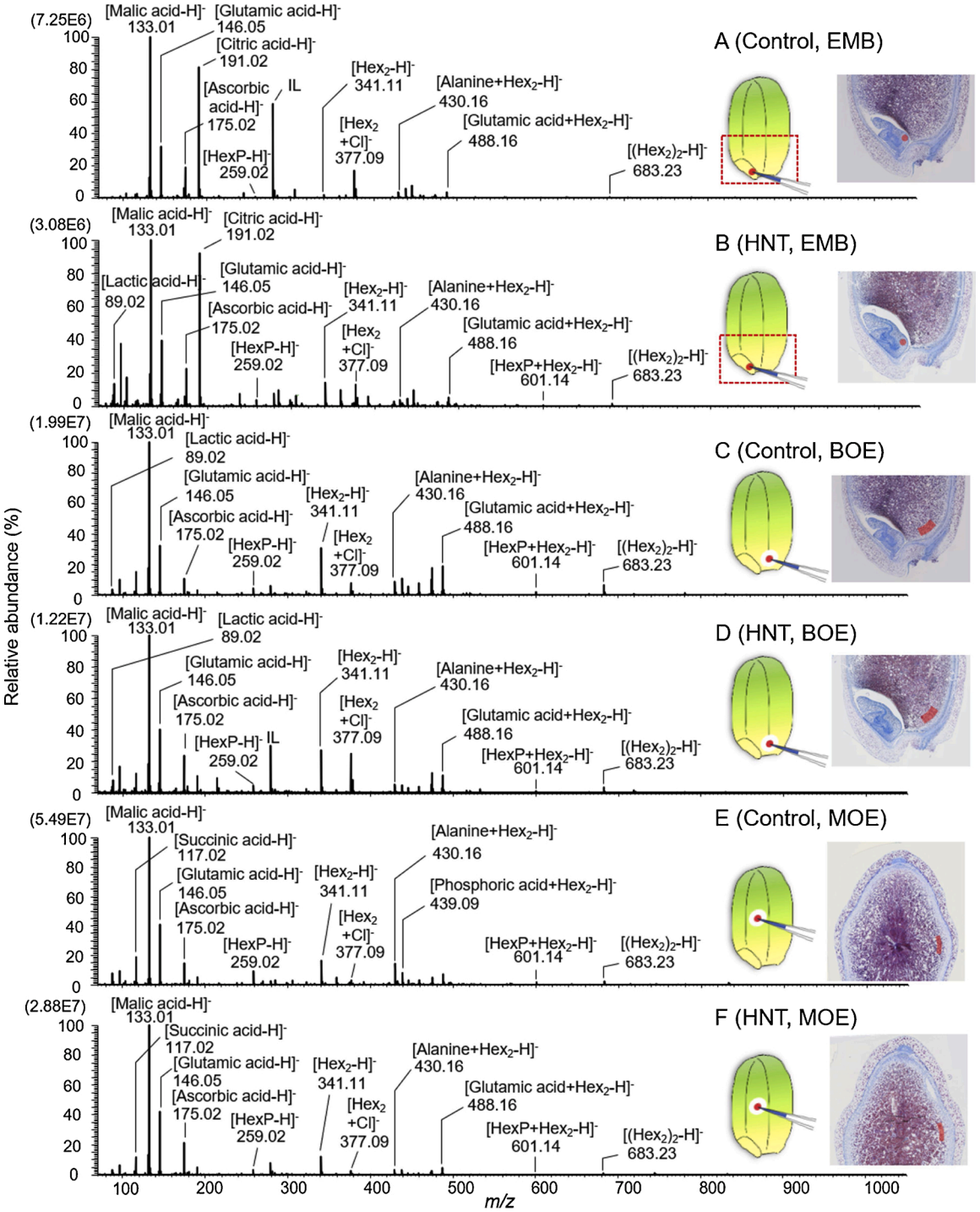

Fig. 3. Negative ion picoPPESI mass spectra obtained from cells of EMB (A and B), BOE (C and D) and MOE (E and F) in control (A, C and E) and HNT treatment (B, D, and F) at 11 DAH. The expanded mass spectra of (B) are shown in Figs. S3–S5. The data are representative of repeated experiments with 3-11 kernels in each treatment. BOE, basal outer endosperm; EMB, embryo; MOE, middle outer endosperm.

3.3. Simultaneous determination of cellular metabolites and redox states in HNT treatment

A number of metabolite signals (130 signals in total) were identified by using picoPPESI-MS in negative ion mode at less than 5 ppm differences from theoretical *m/z* values (Fig. 3, Table S2, also see Figs. S3−5). The peaks assigned to the deprotonated ionic species [malic acid-H]$^-$, [succinic acid-H]$^-$, [glutamic acid-H]$^-$, [ascorbic acid-H]$^-$, and [Hex_2-H]$^-$, were the major signals in each treatment, and there were remarkable site-specific differences in cell composition, including ascorbate-glutathione (ASC-GSH) cycle-related metabolites, sugars and amino acids (Fig. 3, Table S2).

In EMB, [citric acid-H]$^-$ was a major signal, contrastingly different from other two endosperm regions analyzed (Table S2). In HNT treatment, the content of ascorbic acid and dehydroascorbic acid as the [M + Cl]$^-$ species, and lactic acid, allantoin, myristic acid, asparagine and glutamine as [M−H]$^-$ species was significantly higher than in control, whereas the content of deprotonated proline was lower in HNT treatment (Table S2). Most metabolites related to ASC-GSH pathway were prone to be higher in HNT treatment than in control, except for GSSG. The content of [M−H]$^-$ sugar-related signals (with M= Hex, Hex_2, Hex_3, and pentose), the disaccharide cluster $(Hex_2)_2$ as the [M + Cl]$^-$ species, and a series of fatty acids as [M−H]$^-$ were prone to be greater in HNT treatment than control (Figs. 4 and 5 and Table S2).

In BOE, the intensity of deprotonated ions assigned to Hex, Hex_3, pentose, $pentose_2$, ascorbic acid, monodehydroascorbic acid (MDHA), pyruvic acid, fumaric acid, quinic acid, shikimic acid, asparagine, glutamine, sulfuric acid, sulfurous acid, adenine, salicylic acid, and wall-related metabolites, such as UDP-D-xylose/UDP-L-arabinose, D-glucuronic acid and *p*-coumaric acid, and Hex_2 as [M + Cl]$^-$, was significantly higher in HNT treatment than in control, whereas that for leucine/isoleucine, histidine, and tryptophan was lower than in control (Table S2). Overall, the content of metabolites related to TCA cycle, ASC-GSH cycle, most amino acids and cell wall syntheses was observed to be higher in HNT treatment than in control (Figs. 4 and 5).

Contrastingly, in MOE that is presumed to turn to translucent at maturation, the content of succinic acid, valine and threonine was lower in HNT treatment than in control (Table S2). ASC was higher in HNT treatment than in control (Table S2). Except for DHA, the content of ASC-GSH cycle-related metabolites in MOE cells was prone to be higher in HNT treatment than in control; the content of TCA cycle-related metabolites, most amino acids and fatty acids was lower in HNT treatment than in control (Figs. 4 and 5).

The content of redox-related metabolites, ASC, MDHA, DHA, GSH, and GSSG was found to be overall greater in HNT treatment than in control in all regions (Fig. 4). Spatial concentration gradient (i.e., EMB > BOE > MOE) has been observed in each metabolite in HNT treatment, except for GSSG in HNT-treated embryos (Fig. 4). The ASC/DHA ratio in

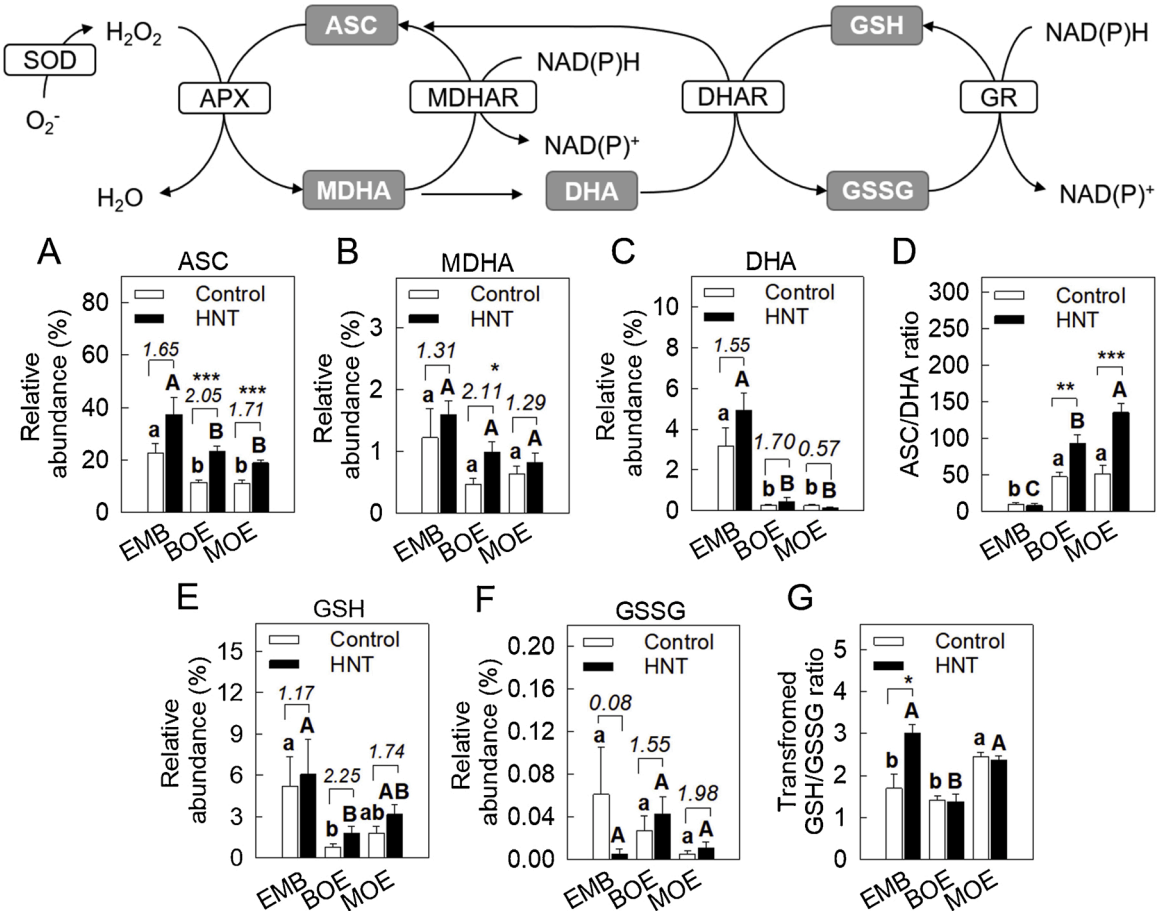

Fig. 4. Ascorbate-glutathione cycle-related metabolites of ASC (A), MDHA (B), DHA (C), the ratio of ASC/DHA (D), GSH (E), GSSG (F) and the ratio of GSH/GSSG (G) detected in the MOE, BOE and EMB in control and HNT treatment. The ratio of GSH/GSSG in MOE, BOE and EMB at each location from each treatment was calculated to be log-transformed (Log (y+1)). The italic values embedded in (A-C) and (E-F) indicate the ratio of HNT to control. ASC, ascorbic acid; APX, ascorbate peroxidase; BOE, basal outer endosperm; DHA, dehydroascorbic acid; DHAR, dehydroascorbate reductase; EMB, embryo; GR, glutathione reductase; GSH, glutathione; GSSG, oxidized glutathione; MDHA, monodehydroascorbic acid; MDHAR, monodehydroascorbate reductase; MOE, middle outer endosperm. Data are the mean ± SE of 3-11 kernels collected from at least three individual plants. Different letters indicate significant differences determined using a Tukey's test to determine the position effect in each treatment. Lowercase and uppercase show control and HNT treatment respectively. *, ** and *** show $p < 0.05$, 0.01 and 0.001 by *t*- test respectively.

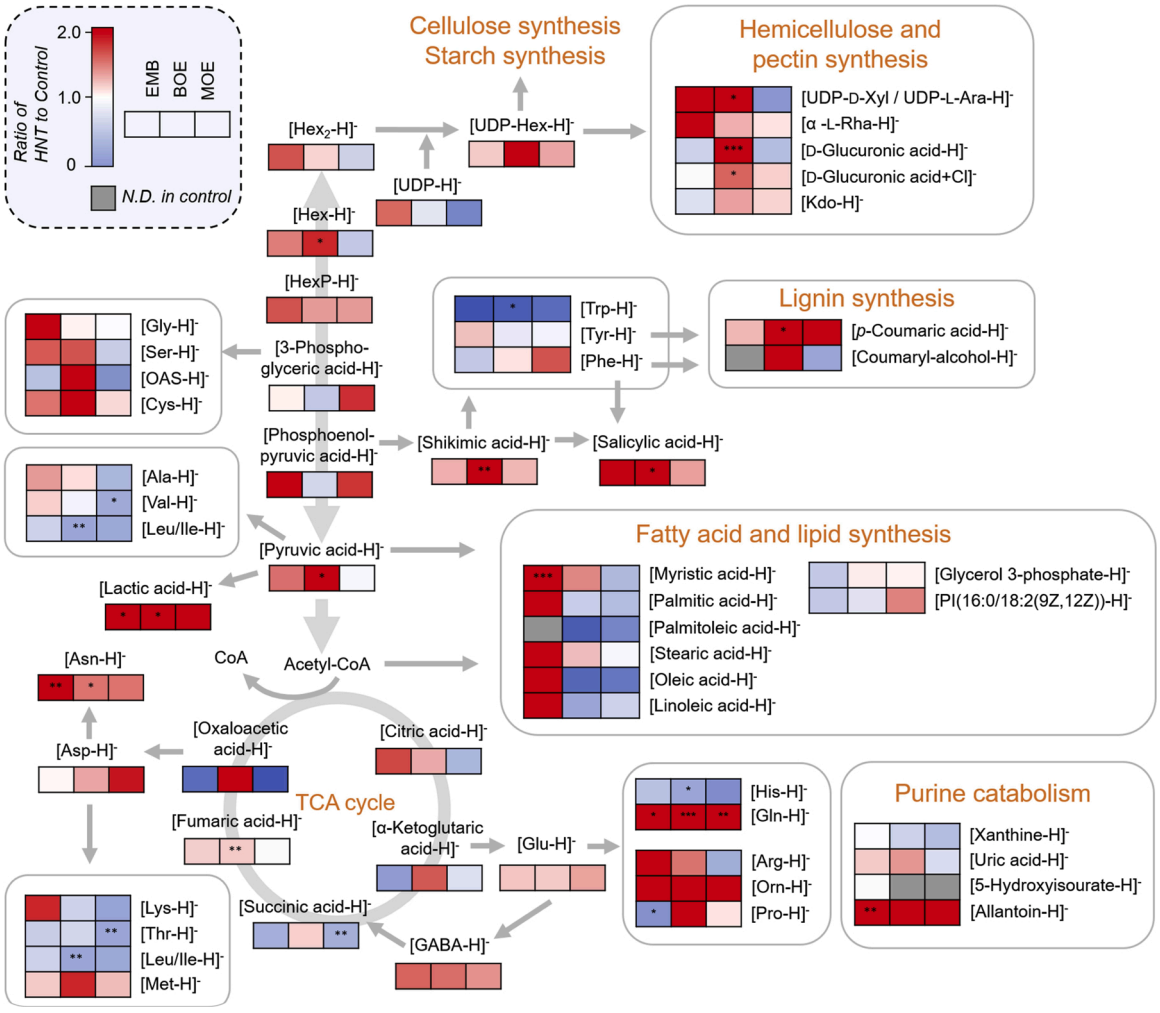

Fig. 5. The metabolites related to glycolysis, TCA cycle, fermentation, amino acids, wall metabolism, purine catabolism, fatty acid and lipid synthesis detected in EMB, BOE and MOE in control and HNT treatment. The ratio of HNT to control in each position is shown by using a color scale (see the upper left). In each box set, EMB, BOE and MOE are aligned from left, center, and right, respectively. α-L-Rha, α-L-rhamnose; Ala, alanine; Arg, arginine; Asn, asparagine; Asp, aspartic acid; BOE, basal outer endosperm; Cys, cysteine; GABA, gamma-aminobutyric acid; EMB, embryo; Gln, glutamine; Glu, glutamic acid; Gly, glycine; His, histidine; Ile, isoleucine; Leu, leucine; Lys, lysine; Met, methionine; MOE, middle outer endosperm; OAS, O-acetylserine; Orn, ornithine; Phe, phenylalanine; Pro, proline; Ser, serine; Trp, tryptophan; Try, tyrosine; UDP, uridine diphosphate; UDP-D-Xyl, uridine diphosphate-D-xylose; UDP-L-Ara, uridine diphosphate-L-arabinose; Val, valine. *, ** and *** show $p < 0.05$, 0.01 and 0.001 by *t*- test respectively. Gray color indicates either not detected or no ratio available due to the zero detection in control.

embryonic scutellum cells was lower than that of endosperms in both treatments (Fig. 4D). In endosperms, the ASC/DHA ratio was prone to be higher in HNT treatment than control, but not for embryonic scutellum cells (Fig. 4D). In HNT-treated endosperms, the ASC/DHA ratio of MOE was greater than that of BOE, exhibiting a considerable difference ($p = 0.05$) (Fig. 4D). In embryonic scutellum cells, there was an increase in GSH/GSSG ratio under HNT conditions (Fig. 4G). The content of lactic acid in HNT-treated embryos was greater than both BOE and MOE (Table S2). Lactic acid also showed spatial concentration gradient in HNT treatment (Table S2). For the content of TCA cycle-related metabolites, opposite patterns were observed between MOE and BOE to in HNT treatment (Fig. 5). Also, glutamine was consistently higher in HNT treatment than in control in all three positions (Fig. 5 and Table S2).

4. Discussion

It is accepted that both ASC and GSH participate in stress response and developmental regulation (Noctor and Foyer, 1998; Noctor et al., 2002; Maughan and Foyer, 2006; Noctor et al., 2012; Akram et al., 2017). These metabolites are considered to be located in cytosol, chloroplast, mitochondria, nucleus, peroxisome, vacuole and apoplastic space (Noctor et al., 2012; Munné-Bosch et al., 2013; Das and Roychoudhury, 2014; Noctor and Foyer, 2016; Bobrovskikh et al., 2020). It has been suggested that glutathione pool and the GSH/GSSG ratio might be two independent systems, and gene expression, protein function and glutathione redox potential might be mostly affected by GSH/GSSG ratio (Noctor et al., 2002). In most biological samples, determination of GSH redox state (expressed as GSH/GSSG ratio) has been made as an indicator of oxidative state by using either colorimetric method (Asensi et al., 1999), LC–MS (Garcia-Quiros et al., 2020) or CE-MS at tissue level (Yamakawa and Hakata, 2010). When collecting the target cells, contamination with neighboring tissues has been a critical issue in any dissection experiment, particularly in the embryo/endosperm interaction studies, as pointed by several investigators (e.g., Doll et al., 2020). An increase in GSH/GSSG ratio was also reported in the pooled rice grains treated under HDT conditions (Yamakawa and Hakata, 2010). To the best of our knowledge, however, no attempt has been made for determining the ratio as well as solute (metabolite) composition at single cell level in real-time.

In the present study, we have directly performed cell-specific metabolome analysis using picoPPESI-MS (Nakashima et al., 2016) to investigate cellular metabolic responses of rice seeds to HNT and its

relation to embryo development (Fig. 2), successfully determining GSH/GSSG and ASC/DHA ratios at the same time. As the results, the spatial patterns of cellular redox states have been revealed in the same grains, as well as remarkable metabolic alterations including a purine catabolism metabolite allantoin, and lactic acid, as discussed below. Except for a reduction in GSSG content in embryonic scutellum cells and DHA in MOE, an overall increase in redox-related metabolites including GSH in all locations has been observed in HNT treatment even during daytime (Fig. 4). Similar reduction in GSSG was also reported in pine embryos at germination (Tommasi et al., 2001). Because ROS scavenging occurs mainly through ASC-GSH cycle (Noctor and Foyer, 1998; Foyer and Noctor, 2011), our data suggest that maintaining a certain level of ROS might be essential for the active cell expansion observed in HNT-treated embryonic cells (Figs. 2 and 4). And, it is very likely that the marked increase in cellular GSH/GSSG ratio due to a decrease in GSSG content (Fig. 4; Table S2) might optimize cellular metabolisms during expansion by regulating cellular redox homeostasis.

HNT-treated rice plants are subjected to mild shoot water deficit at night (Wada et al., 2021), although it is expected that plant water status might be recovering during daytime and there would be less influence of water deficit in the day, compared with nighttime. PicoPPESI-MS analysis was performed during daytime due to the technical demandingness; however, even so, our analysis has revealed that HNT treatment induced greater accumulation of sugars, allantoin, glutamine, and lactic acid in the growing embryos during daytime as the history of HNT treatment (Fig. 5, Table S2). During the cell pressure probe operation, the probe tip was assumed to reach to the vacuoles through a part of cytosolic space after tip impalement into the target cells (Steudle, 1993; Murphy and Smith, 1998). Based on the anatomical data (Figs. 2, S1 and S2), cellular fluids we collected in the probe tip would be regarded as the mixture of vacuoles and cytosolic compartment containing organelles, such as mitochondria, peroxisomes, and plastids, as addressed below. The detection of metabolites related to ASC-GSH cycle in this study has implied the abundance of these metabolites in the cells.

It is suggested that seeds under hypoxia status may lead accumulation of lactate and decreasing of ATP level in legumes (Rolletschek et al., 2003). In this study, ATP signal itself has not been detected, possibly due to its rapid turnover and/or the relatively low concentration in the cell. However, substantial lactic acid accumulation detected at HNT (see Fig. 5 and Table S2) has implied that BOE might have encountered a more severe hypoxia environment in HNT treatment, compared with MOE. According to the observed changes in TCA cycle-related metabolites (Fig. 5), it has been suggested that an inhibition of respiration chain (Yamakawa and Hakata, 2010) or some impairment of mitochondria might have been caused by HNT. Greater accumulation of lactic acid observed here suggests the promotion of fermentation under HNT condition. In addition to lactic acid, sugars detected as Hex, Hex_2 ($[M + Cl]^-$), greater content of pentose, $pentose_2$ ($p = 0.07$), cysteine ($p = 0.198$), organic acids (pyruvic acid, fumaric acid, quinic acid, shikimic acid), sulfurous acid, and wall-related metabolites, such as UDP-Hex and UDP-D-xyl/UDP-L-Ara, have been detected in HNT-treated BOE with an increase in ASC and MDHA as typical HNT responses, presumably optimizing cellular redox states (Figs. 4 and 5, Table S2).

In addition to the increase in GSH/GSSG ratio detected in embryonic cells, our picoPPESI-MS analysis has identified an increase in ASC/DHA ratio in the endosperms in response to HNT treatment. An increasing in the content of ASC and activity of ascorbate peroxidase may be associated with delayed programmed cell death (PCD) in wheat endosperms under non-stress conditions (Paradiso et al., 2012). In addition, it has been reported that the overexpression of dehydroascorbate reductase (DHAR) with enhancing ASC and ASC/DHA ratio could work protection against heat-induced oxidative stress in *Arabidopsis* seedling (Wang et al., 2010). In this study, the exact role(s) on ASC (and ASC/DHA ratio) on embryo and endosperm development remains obscure partially due to the lack of time-course analysis; however, it should be emphasized that there was a difference in the ASC/DHA ratio between BOE and MOE even in the same endosperms (see Results). This difference may refer to the fate of each region prior to maturation, as the BOE and MOE regions turned to chalk and translucent until harvest, respectively under HNT conditions (Figs. 1 and 4). In this view, it is expected that sustaining a high ASC/DHA ratio might be the prerequisite for alleviating the occurrence of chalkiness under HNT. Alternatively, this may imply the presence of threshold for ASC/DHA ratio in terms of chalky formation.

During maize endosperm development, ethylene may play a role on the regulation of PCD (Young et al., 1997). In maize, PCD initiated from the central endosperm in both wild type and *shrunken2 (sh2)* genotype, although compared with wild type the speed of cell death and DNA fragmentation was faster in *sh2* kernels that showed higher content of ethylene precursor, 1-aminocyclopropane-1-carboxylic acid (ACC) and ethylene production rate (Young et al., 1997). Therefore, one may expect that there may be a possible interaction between PCD and ACC. When ACC was assayed at two different positions in the same outer rice endosperms in this study, there was no difference in ACC content between the cells (see MOE and BOE in Table S2). Based on the data, it is likely that ethylene synthesis may not be relevant in the cells targeted here. And hence, same interpretation with ACC may not be applicable for at least the rice endosperms in this study. Hence, it is presumed that ASC might be associated with chalky formation in the outer endosperm as a heat acclimation under HNT conditions, rather than PCD regulation.

In rice and barley, it has been reported that endosperm sugar accumulation also affects ABA signaling and a reduction in starch synthesis rate may break embryonic dormancy to induce pre-harvest sprouting (PHS) (Howard et al., 2012; Du et al., 2018). More recently, Xu et al. have shown that *PHS9* gene might be involved in ABA signaling as a negative regulator during the late stage of seed development in rice (Xu et al., 2019). They also reported that *PHS9* encoding one of the CC-type glutaredoxins is expressed in embryos at late stage of seed development and induced by H_2O_2 and ABA (Xu et al., 2019). Because glutaredoxins are closely associated with cellular redox homoeostasis controlling the GSH/GSSG ratio, the results shown in Fig. 4G may refer to the consequence of site-specific activation of the enzyme. In addition, this cellular response may be closely associated with some epigenetic modification that might occur in HNT-treated embryos, as discussed below.

Purine catabolism is known to undergo in peroxisome from the process of transforming uric acid to allantoin, accompanying with the H_2O_2 production. And then, allantoin is transported to endoplasmic reticulum (ER) to form glyoxylate by releasing NH_3 for nitrogen re-usage (Zrenner et al., 2006; Corpas et al., 2017; Watanabe and Sakamoto, 2018). We have also detected high concentration of allantoin in the embryonic cells actively growing in HNT treatment (Table S2). Therefore, it has been suggested that peroxisomes were highly contaminated as major organelle(s) contaminated in the cellular fluids collected and allantoin transport from peroxisome to ER is very likely to be inhibited without consuming water molecules in the downstream of pathway in ER. Also, there was no detection for ABA signals at least at the stage analyzed (i.e., 11DAH), and thus it remains questionable whether allantoin is associated with ABA response in HNT treatment. However, similar to ASC and other redox-related molecules in the peroxisome, allantoin may serve an antioxidant under abiotic stress (Brychkova et al., 2008; Watanabe and Sakamoto, 2018). Taken these together, it has been shown that metabolic regulations, particularly redox states and energy status (fermentation and TCA cycle) would be tightly coordinated within seeds at HNT (Figs. 1, 4 and 5).

In addition to the acceleration of embryo growth, HNT simultaneously causes a diminishment of endosperm cell size (Morita et al., 2005; Wada et al., 2021) and basal chalky formation (see Figs. 1 and 2). Regarding chalky formation, there is accumulating evidence that vacuolar compartments remaining in cytosol may take part in the air space formation under heat-like stress conditions, resulting in chalky formation (for white belly and white core rice, Li et al., 2014; white-back rice, Wada et al., 2019; ring-shaped chalkiness, called milky-white rice, Hatakeyama et al., 2018), accompanying with a partial inhibition of

starch (and protein) accumulation. There might be a relation between an impairment in mitochondria and chalky formation, although this remains to be investigated further. More recently, a possible interaction between chalky formation and embryo development at HDT has been pointed (Wada et al., 2019; An et al., 2020), although any clear relationship has not been established yet. Microscopic observations (see Fig. S2) reveal a similar role of preserved cytosolic space, mainly composed of vacuolar compartments with respect to the basal chalky formation, suggesting that basal chalky formation may be similarly explained. At 11 DAH, where picoPPESI-MS was conducted, organ differentiation had been completed and embryonic growth is attributed to cell enlargement (see insets in Figs. 2K and 6) (Itoh et al., 2005). It is noteworthy that embryonic cell enlargement was synchronized with a reduction in gap (cytosolic) space in basal endosperm cells in both treatments (Fig. S6A). The analysis suggests that the relative rate of embryonic cell expansion was correlated with the relative gap size reduction rate in the basal endosperms, exhibiting a clear sift (Fig. S6B). This represents that there is a close relationship between embryo growth and chalky formation, as previously proposed in heat-induced chalky formation (Wada et al., 2019).

A loss of kernel DW and an increase in embryo DW measured in HNT treatment was ca. 1.5 mg and 0.08 mg, respectively (Fig. 2A and B). Dry weight loss in the chalky zone in HNT treatment corresponds to 11.02 % of total grain DW (Wada et al., 2021). If we assume that same amount of assimilates was supplied into the embryos, a decline in dry matter in chalky region should correspond to 48.5 % (= 0.08/0.165 × 100) of the dry matter used for embryo development. However, this value might be overestimated because the dependence on dry matter once stored in the

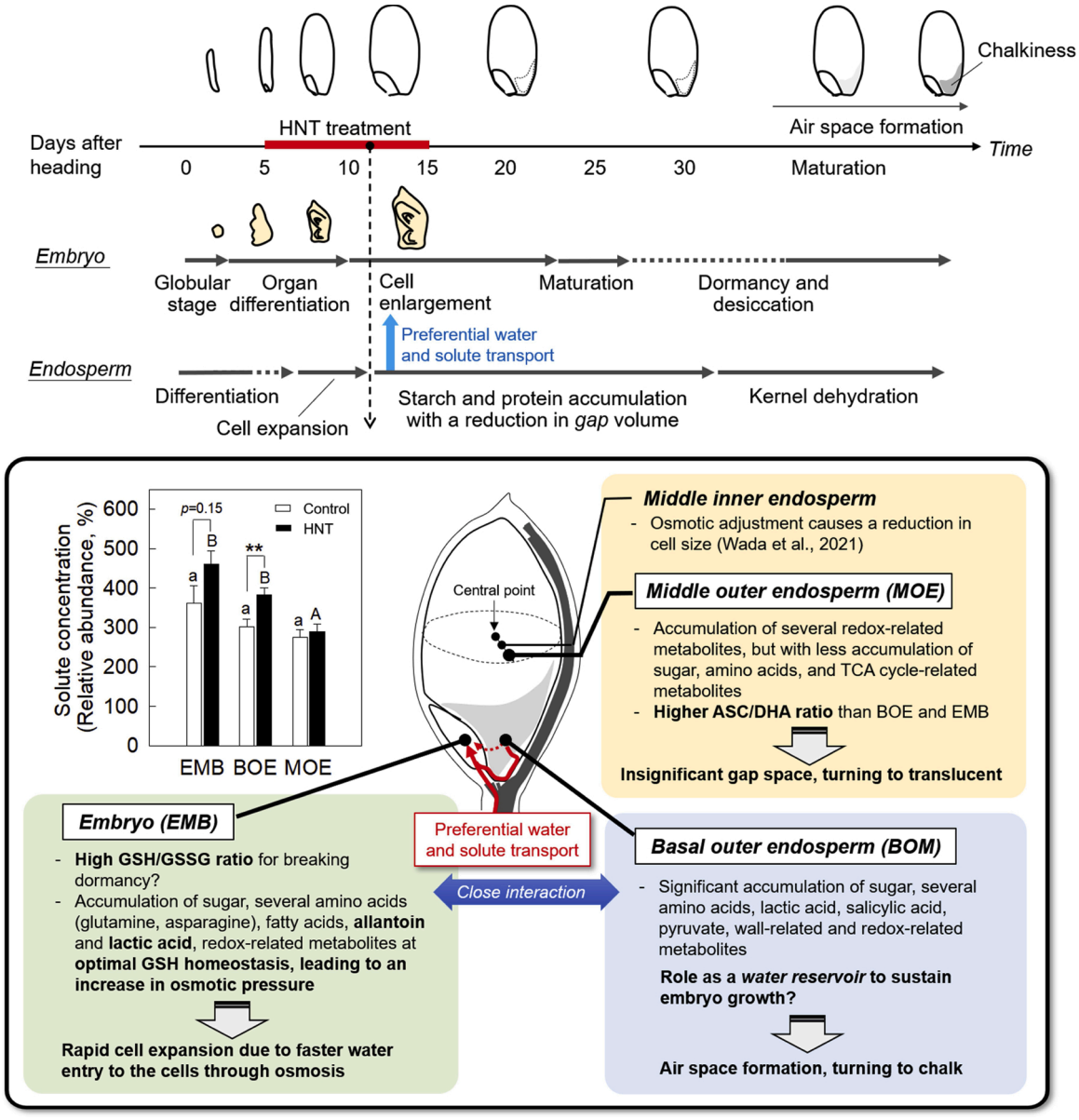

Fig. 6. Schematic diagrams of rice seed development and morphological events occurring at embryo and endosperm in the developing 'Koshihikari' kernels under HNT conditions. The below indicates a summary of the cell-specific events and related major metabolic alterations observed at each location (embryos and middle and basal endosperms) at 11 DAH during HNT treatment shown in red. The inset figure shows solute concentration estimated as the cumulative relative abundance of all signals detected in negative ion mode. Significant treatment differences were observed in EMB and BOE at $p < 0.15$ and $p < 0.01$ (shown by **) by *t*-test, respectively. The cell metabolomics (Figs. 3–5) and morphological image analysis (see Fig. S6) data have suggested that there was a close relationship between the acceleration of embryo development under HNT conditions and basal chalky formation. It is proposed that preferential water and solute transport between these organs may contribute to the rapid embryo enlargement (see Discussion).

endosperms would become larger as HNT duration extends. Because of the technical limitations, positive ion MS and cell osmotic pressure were not determined in this study. However, when cumulative relative abundance of metabolites detected here (Table S2) was estimated as total solute concentration, the values in EMB and BOM cells in HNT treatment were prone to be higher than control (Fig. 6). One plausible explanation for this is that embryonic cells in HNT treatment would have been under more concentrated conditions than control. If this were the case, then the increase in cell osmotic pressure would induce preferential water entry into the embryo from xylem and endosperm cells through possible pathways including along the central line to promote embryonic cell expansion at HNT, leading to the acceleration of embryo development (see Fig. 2). This is what we observed in the inset of Fig. 6. High concentration of sugars and amino acids detected in the endosperm cells in the vicinity of developing embryos supports this suggestion (Fig. 4, Table S2). Since cell hydraulic conductivity is also affected by redox state (Henzler and Steudle, 2000), redox regulation at an optimal ROS concentration may play a central role for water transport to the embryos. In this view, cytosolic (vacuolar) water stored in the basal endosperm cells may be partially contribute to the germination, as previously proposed (Wada et al., 2019)

Recent studies have shown that epigenetic modification plays a crucial role on rice seed development through double fertilization process (Zemach et al., 2010). Given into the fact that redox state and glutathione are known to participate in epigenetic modifications, including DNA methylation, histone acetylation, histone methylation and histone glutathionylation (Shen et al., 2016; Locato et al., 2018), it is possible that some epigenetic modifications might occur under HNT conditions. In addition, ROS is known to participate in seed dormancy breaking and seedling establishment in rice (Zhou et al., 2018). More recently, it has been proposed that hormonal signaling is involved in the spatiotemporal regulation of ROS production for cell expansion associated with seed germination (Bailly, 2019). By assaying cellular metabolites in BOE at the maximum embryonic cell expansion stage using picoPPESI-MS (Figs. 3–5), several similarities including redox regulation have been observed between HNT- and HDT-treated endosperms (i.e., white-back rice formation) (Wada et al., 2019). There was no detection for the candidate hormones, such as GA and ABA. However, these discrepancies may be attributed to the differences in stages, although this awaits future study.

5. Conclusion

We have site-specifically assayed metabolic responses to HNT treatment in the developing grains by utilizing picoPPESI-MS. Considerable solute accumulation including redox-related metabolites and allantoin has been successfully characterized at cell level in both embryos and two locations of endosperms under HNT conditions. The role of ASC/DHA ratio might be involved in the formation of chalkiness under HNT treatment. The cellular determination of relative intensity-based GSH/GSSG ratio has suggested that acceleration of embryo growth may be closely associated with the optimization of redox state in HNT treatment. Since GSH oxidative state is known to be prerequisite of dormancy alleviation, controlling an optimal redox homeostasis observed in embryos would lead to an acceleration of embryo growth in developing seeds observed under HNT conditions. As shown here, simultaneous determination of GSH/GSSG and ASC/DHA ratios was attainable at cell level in HNT-treated ‘Koshihikari’ seeds using picoPPESI-MS. And hence, this analytical method may also be applicable to other biological samples. When considering the relatively large cultivar-to-cultivar variation on rice seed anatomy, it is anticipated that conducting the same analysis for the varietal difference might be challenging. Further research on the varietal difference including this method may provide useful information for rice breeding strategies in order to cope with nighttime warming.

Author contributions

F.-Y.C. and H.W. conceived the study. F.-Y.C. and Y.H. performed the experiments, and F.Y.-C. analyzed data. F.-Y.C. and H.W. prepared the manuscript. Y.H., H.No., R.E.-B., T.A. and H.Na. participated in analysis of data and assisted in writing the manuscript. All authors read and approved the manuscript.

Data availability

The datasets generated during and/or analyzed during the current study are available from the corresponding author on reasonable request.

Declaration of Competing Interest

The authors report no declarations of interest.

Acknowledgments

The authors thank Ms. Fujiko Komiya for her help in growing the rice plants and assistance with the experiments. R.E.-B. is research member of National Council of Scientific and Technological Research (CONICET), Argentina. This work was supported by JSPS KAKENHI Grant Number 16H02533. F.-Y.C. thanks the scholarship from “Agricultural Elitist Training Project” of Council of Agriculture, Executive Yuan, Taiwan.

Appendix A. Supplementary data

Supplementary material related to this article can be found, in the online version, at doi:https://doi.org/10.1016/j.envexpbot.2021.104515.

References

Akram, N.A., Shafiq, F., Ashraf, M., 2017. Ascorbic acid-a potential oxidant scavenger and its role in plant development and abiotic stress tolerance. Front. Plant Sci. 8 https://doi.org/10.3389/fpls.2017.00613.

An, L., Tao, Y., Chen, H., He, M., Xiao, F., Li, G., Ding, Y., Liu, Z., 2020. Embryo-endosperm interaction and its agronomic relevance to rice quality. Front. Plant Sci. 11 https://doi.org/10.3389/fpls.2020.587641.

Asensi, M., Sastre, J., Pallardo, F.V., Lloret, A., Lehner, M., Garcia-de-la Asuncion, J., Vina, J., 1999. Ratio of reduced to oxidized glutathione as indicator of oxidative stress status and DNA damage. Methods Enzymol. 299, 267–276. https://doi.org/10.1016/S0076-6879(99)99026-2.

Bailly, C., 2019. The signalling role of ROS in the regulation of seed germination and dormancy. Biochem. J. 476, 3019–3032. https://doi.org/10.1042/BCJ20190159.

Bobrovskikh, A., Zubairova, U., Kolodkin, A., Doroshkov, A., 2020. Subcellular compartmentalization of the plant antioxidant system: an integrated overview. PeerJ 8, e9451. https://doi.org/10.7717/peerj.9451.

Brunel-Muguet, S., D'Hooghe, P., Bataille, M.P., Larre, C., Kim, T.H., Trouverie, J., Avice, J.C., Etienne, P., Durr, C., 2015. Heat stress during seed filling interferes with sulfur restriction on grain composition and seed germination in oilseed rape (*Brassica napus* L.). Front. Plant Sci. 6, 213. https://doi.org/10.3389/fpls.2015.00213.

Brychkova, G., Alikulov, Z., Fluhr, R., Sagi, M., 2008. A critical role for ureides in dark and senescence-induced purine remobilization is unmasked in the *Atxdh1* Arabidopsis mutant. Plant J. 54, 496–509. https://doi.org/10.1111/j.1365-313X.2008.03440.x.

Corpas, F.J., Barroso, J.B., Palma, J.M., Rodriguez-Ruiz, M., 2017. Plant peroxisomes: a nitro-oxidative cocktail. Redox Biol. 11, 535–542. https://doi.org/10.1016/j.redox.2016.12.033.

Das, K., Roychoudhury, A., 2014. Reactive oxygen species (ROS) and response of antioxidants as ROS-scavengers during environmental stress in plants. Front. Environ. Sci. 2 https://doi.org/10.3389/fenvs.2014.00053.

Doll, N.M., Just, J., Brunaud, V., Caius, J., Grimault, A., Depege-Fargeix, N., Esteban, E., Pasha, A., Provart, N.J., Ingram, G.C., Rogowsky, P.M., Widiez, T., 2020. Transcriptomics at maize embryo/endosperm interfaces identifies a transcriptionally distinct endosperm subdomain adjacent to the embryo scutellum. Plant Cell 32, 833–852. https://doi.org/10.1105/tpc.19.00756.

Du, L., Xu, F., Fang, J., Gao, S., Tang, J., Fang, S., Wang, H., Tong, H., Zhang, F., Chu, J., Wang, G., Chu, C., 2018. Endosperm sugar accumulation caused by mutation of *PHS8/ISA1* leads to pre-harvest sprouting in rice. Plant J. 95, 545–556. https://doi.org/10.1111/tpj.13970.

El-Maarouf-Bouteau, H., Meimoun, P., Job, C., Job, D., Bailly, C., 2013. Role of protein and mRNA oxidation in seed dormancy and germination. Front. Plant Sci. 4, 77. https://doi.org/10.3389/fpls.2013.00077.

Foyer, C.H., Noctor, G., 2011. Ascorbate and glutathione: the heart of the redox hub. Plant Physiol. 155, 2–18. https://doi.org/10.1104/pp.110.167569.

Garcia-Quiros, E., Alche, J.D., Karpinska, B., Foyer, C.H., 2020. Glutathione redox state plays a key role in flower development and pollen vigour. J. Exp. Bot. 71, 730–741. https://doi.org/10.1093/jxb/erz376.

Hatakeyama, Y., Masumoto-Kubo, C., Nonami, H., Morita, S., Hiraoka, K., Onda, Y., Nakashima, T., Nakano, H., Wada, H., 2018. Evidence for preservation of vacuolar compartments during foehn-induced chalky ring formation of *Oryza sativa* L. Planta 248, 1263–1275. https://doi.org/10.1007/s00425-018-2975-x.

Henzler, T., Steudle, E., 2000. Transport and metabolic degradation of hydrogen peroxide in *Chara corallina*: model calculations and measurements with the pressure probe suggest transport of H_2O_2 across water channels. J. Exp. Bot. 51, 2053–2066. https://doi.org/10.1093/jexbot/51.353.2053.

Hoshikawa, K., 1989. The Growing Rice Plant: An Anatomical Monograph. Nosan Gyoson Bunka Kyokai, Tokyo.

Howard, T.P., Fahy, B., Craggs, A., Mumford, R., Leigh, F., Howell, P., Greenland, A., Smith, A.M., 2012. Barley mutants with low rates of endosperm starch synthesis have low grain dormancy and high susceptibility to preharvest sprouting. New Phytol. 194, 158–167. https://doi.org/10.1111/j.1469-8137.2011.04040.x.

IPCC, 2013. Climate change 2013: the physical science basis. In: Stocker, T.F., Qin, D., Plattner, G.K., Tignor, M., Allen, S.K., Boschung, J., Nauels, A., Xia, Y., Bex, V., Midgley, P.M. (Eds.), Contribution of Working Group I to the Fifth Assessment Report of the Intergovernmental Panel on Climate Change. Cambridge University Press, Cambridge, United Kingdom and New York.

Itoh, J.-I., Nonomura, K.-I., Ikeda, K., Yamaki, S., Inukai, Y., Yamagishi, H., Kitano, H., Nagato, Y., 2005. Rice plant development: from zygote to spikelet. Plant Cell Physiol. 46, 23–47. https://doi.org/10.1093/pcp/pci501.

Jagadish, S.V.K., Murty, M.V.R., Quick, W.P., 2015. Rice responses to rising temperatures-challenges, perspectives and future directions. Plant Cell Environ. 38, 1686–1698. https://doi.org/10.1111/pce.12430.

Kobayashi, A., Hori, K., Yamamoto, T., Yano, M., 2018. Koshihikari: a premium short-grain rice cultivar – its expansion and breeding in Japan. Rice (N. Y.) 11, 15. https://doi.org/10.1186/s12284-018-0207-4.

Li, Y., Fan, C., Xing, Y., Yun, P., Luo, L., Yan, B., Peng, B., Xie, W., Wang, G., Li, X., Xiao, J., Xu, C., He, Y., 2014. *Chalk5* encodes a vacuolar H^+-translocating pyrophosphatase influencing grain chalkiness in rice. Nat. Genet. 46, 398–404. https://doi.org/10.1038/ng.2923.

Locato, V., Cimini, S., De Gara, L., 2018. ROS and redox balance as multifaceted players of cross-tolerance: epigenetic and retrograde control of gene expression. J. Exp. Bot. 69, 3373–3391. https://doi.org/10.1093/jxb/ery168.

Maughan, S., Foyer, C.H., 2006. Engineering and genetic approaches to modulating the glutathione network in plants. Physiol. Plant. 126, 382–397. https://doi.org/10.1111/j.1399-3054.2006.00684.x.

Morita, S., Shiratsuchi, H., Takahashi, J., Fujita, K., 2004. Effect of high temperature on grain ripening in rice plants: analysis of the effects of high night and high day temperatures applied to the panicle and other parts of the plant (in Japanese with English abstract). Jpn. J. Crop Sci. 73, 77–83. https://doi.org/10.1626/jcs.73.77.

Morita, S., Yonemaru, J., Takanashi, J., 2005. Grain growth and endosperm cell size under high night temperatures in rice (*Oryza sativa* L.). Ann. Bot. 95, 695–701. https://doi.org/10.1093/aob/mci071.

Morita, S., Wada, H., Matsue, Y., 2016. Countermeasures for heat damage in rice grain quality under climate change. Plant Prod. Sci. 19, 1–11. https://doi.org/10.1080/1343943X.2015.1128114.

Munné-Bosch, S., Queval, G., Foyer, C.H., 2013. The impact of global change factors on redox signaling underpinning stress tolerance. Plant Physiol. 161, 5–19. https://doi.org/10.1104/pp.112.205690.

Murphy, R., Smith, J.A.C., 1998. Determination of cell water-relation parameters using the pressure probe: extended theory and practice of the pressure-clamp technique. Plant Cell Environ. 21, 637–657. https://doi.org/10.1046/j.1365-3040.1998.00316.x.

Nakashima, T., Wada, H., Morita, S., Erra-Balsells, R., Hiraoka, K., Nonami, H., 2016. Single-cell metabolite profiling of stalk and glandular cells of intact trichomes with internal electrode capillary pressure probe electrospray ionization mass spectrometry. Anal. Chem. 88, 3049–3057. https://doi.org/10.1021/acs.analchem.5b03366.

Noctor, G., Foyer, C.H., 1998. Ascorbate and glutathione: keeping active oxygen under control. Annu. Rev. Plant Physiol. Plant Mol. Biol. 49, 249–279. https://doi.org/10.1146/annurev.arplant.49.1.249.

Noctor, G., Foyer, C.H., 2016. Intracellular redox compartmentation and ROS-related communication in regulation and signaling. Plant Physiol. 171, 1581–1592. https://doi.org/10.1104/pp.16.00346.

Noctor, G., Gomez, L., Vanacker, H.l.n., Foyer, C.H., 2002. Interactions between biosynthesis, compartmentation and transport in the control of glutathione homeostasis and signalling. J. Exp. Bot. 53, 1283–1304. https://doi.org/10.1093/jxb/53.372.1283.

Noctor, G., Mhamdi, A., Chaouch, S., Han, Y., Neukermans, J., Marquez-garcia, B., Queval, G., Foyer, C.H., 2012. Glutathione in plants: an integrated overview. Plant Cell Environ. 35, 454–484. https://doi.org/10.1111/j.1365-3040.2011.02400.x.

Oracz, K., El-Maarouf Bouteau, H., Farrant, J.M., Cooper, K., Belghazi, M., Job, C., Job, D., Corbineau, F., Bailly, C., 2007. ROS production and protein oxidation as a novel mechanism for seed dormancy alleviation. Plant J. 50, 452–465. https://doi.org/10.1111/j.1365-313X.2007.03063.x.

Paradiso, A., de Pinto, M.C., Locato, V., De Gara, L., 2012. Galactone-γ-lactone-dependent ascorbate biosynthesis alters wheat kernel maturation. Plant Biol. 14, 652–658. https://doi.org/10.1111/j.1438-8677.2011.00543.x.

Peng, S., Huang, J., Sheehy, J.E., Laza, R.C., Visperas, R.M., Zhong, X., Centeno, G.S., Khush, G.S., Cassman, K.G., 2004. Rice yields decline with higher night temperature from global warming. Proc. Natl. Acad. Sci. U. S. A. 101, 9971–9975. https://doi.org/10.1073/pnas.0403720101.

Rolletschek, H., Weber, H., Borisjuk, L., 2003. Energy status and its control on embryogenesis of legumes. Embryo photosynthesis contributes to oxygen supply and is coupled to biosynthetic fluxes. Plant Physiol. 132, 1196–1206. https://doi.org/10.1104/pp.102.017376.

Saito, Y., Shigemitsu, T., Tanaka, K., Morita, S., Satoh, S., Masumura, T., 2010. Ultrastructure of mature protein body in the starchy endosperm of dry cereal grain. Biosci. Biotechnol. Biochem. 74, 1485–1487. https://doi.org/10.1271/bbb.100147.

Shen, Y., Issakidis-Bourguet, E., Zhou, D.-X., 2016. Perspectives on the interactions between metabolism, redox, and epigenetics in plants. J. Exp. Bot. 67, 5291–5300. https://doi.org/10.1093/jxb/erw310.

Shi, W., Yin, X., Struik, P.C., Solis, C., Xie, F., Schmidt, R.C., Huang, M., Zou, Y., Ye, C., Jagadish, S.V.K., 2017. High day- and night-time temperatures affect grain growth dynamics in contrasting rice genotypes. J. Exp. Bot. 68, 5233–5245. https://doi.org/10.1093/jxb/erx344.

Steudle, E., 1993. Pressure probe techniques: basic principles and application to studies of water and solute relations at the cell, tissue and organ level. In: Smith, J.A.C., Griffiths, H. (Eds.), Water Deficits: Plant Responses from Cell to Community. Bios Scientific Publishers, Oxford, UK, pp. 5–36.

Suriyasak, C., Harano, K., Tanamachi, K., Matsuo, K., Tamada, A., Iwaya-Inoue, M., Ishibashi, Y., 2017. Reactive oxygen species induced by heat stress during grain filling of rice (*Oryza sativa* L.) are involved in occurrence of grain chalkiness. J. Plant Physiol. 216, 52–57. https://doi.org/10.1016/j.jplph.2017.05.015.

Tommasi, F., Paciolla, C., de Pinto, M.C., Gara, L.D., 2001. A comparative study of glutathione and ascorbate metabolism during germination of *Pinus pinea* L. seeds. J. Exp. Bot. 52, 1647–1654. https://doi.org/10.1093/jxb/52.361.1647.

Wada, H., 2019. New approaches combined with environmental control for enhancing heat-tolerant rice breeding in Japan (Chapter 3). In: Iizumi, T., Hirata, R., Matsuda, R. (Eds.), Adaptation to Climate Change in Agriculture. Springer, Singapore, pp. 37–51. https://doi.org/10.1007/978-981-13-9235-1_3.

Wada, H., Nonami, H., Yabuoshi, Y., Maruyama, A., Tanaka, A., Wakamatsu, K., Sumi, T., Wakiyama, Y., Ohuchida, M., Morita, S., 2011. Increased ring-shaped chalkiness and osmotic adjustment when growing rice grains under foehn-induced dry wind condition. Crop Sci. 51, 1703–1715. https://doi.org/10.2135/cropsci2010.08.0503.

Wada, H., Hatakeyama, Y., Onda, Y., Nonami, H., Nakashima, T., Erra-Balsells, R., Morita, S., Hiraoka, K., Tanaka, F., Nakano, H., 2019. Multiple strategies for heat adaptation to prevent chalkiness in the rice endosperm. J. Exp. Bot. 70, 1299–1311. https://doi.org/10.1093/jxb/ery427.

Wada, H., Chang, F.-Y., Hatakeyama, Y., Erra-Balsells, R., Araki, T., Nakano, H., Nonami, H., 2021. Endosperm cell size reduction caused by osmotic adjustment during nighttime warming in rice. Sci. Rep. 11, 4447. https://doi.org/10.1038/s41598-021-83870-1.

Wang, Z., Xiao, Y., Chen, W., Tang, K., Zhang, L., 2010. Increased vitamin C content accompanied by an enhanced recycling pathway confers oxidative stress tolerance in *Arabidopsis*. J. Integr. Plant Biol. 52, 400–409. https://doi.org/10.1111/j.1744-7909.2010.00921.x.

Watanabe, S., Sakamoto, A., 2018. Plant purine catabolism-recent advances and the emerging role in stress adaptation (in Japanese with English abstract). Rel. Plant Growth Dev. 53, 116–123. https://doi.org/10.18978/jscrp.53.2_116.

WMO, 2020. The State of Greenhouse Gases in the Atmosphere Based on Global Observations through 2019. WMO Greenhouse Gas Bulletin (GHG Bulletin) No. 16. https://reliefweb.int/report/world/wmo-greenhouse-gas-bulletin-state-greenhouse-gases-atmosphere-based-global-1 (Accessed 23 November 2020). World Meteorological Organization.

Wu, Y.-C., Chang, S.-J., Lur, H.-S., 2016. Effects of field high temperature on grain yield and quality of a subtropical type *japonica* rice—Pon-Lai rice. Plant Prod. Sci. 19, 145–153. https://doi.org/10.1080/1343943X.2015.1128091.

Xu, F., Tang, J., Gao, S., Cheng, X., Du, L., Chu, C., 2019. Control of rice pre-harvest sprouting by glutaredoxin-mediated abscisic acid signaling. Plant J. 100, 1036–1051. https://doi.org/10.1111/tpj.14501.

Xu, J., Henry, A., Sreenivasulu, N., 2020. Rice yield formation under high day and night temperatures-a prerequisite to ensure future food security. Plant Cell Environ. 43, 1595–1608. https://doi.org/10.1111/pce.13748.

Yamakawa, H., Hakata, M., 2010. Atlas of rice grain filling-related metabolism under high temperature: joint analysis of metabolome and transcriptome demonstrated inhibition of starch accumulation and induction of amino acid accumulation. Plant Cell Physiol. 51, 795–809. https://doi.org/10.1093/pcp/pcq034.

Young, T.E., Gallie, D.R., DeMason, D.A., 1997. Ethylene-mediated programmed cell death during maize endosperm development of wild-type and *shrunken2* genotypes. Plant Physiol. 115, 737–751. https://doi.org/10.1104/pp.115.2.737.

Zemach, A., Kim, M.Y., Silva, P., Rodrigues, J.A., Dotson, B., Brooks, M.D., Zilberman, D., 2010. Local DNA hypomethylation activates genes in rice endosperm. Proc. Natl. Acad. Sci. U. S. A. 107, 18729–18734. https://doi.org/10.1073/pnas.1009695107.

Zhou, L., Ye, Y., Zhao, Q., Du, X., Zakari, S.A., Su, D., Pan, G., Cheng, F., 2018. Suppression of ROS generation mediated by higher $InsP_3$ level is critical for the delay of seed germination in *lpa* rice. Plant Growth Regul. 85, 411–424. https://doi.org/10.1007/s10725-018-0402-8.

Zrenner, R., Stitt, M., Sonnewald, U., Boldt, R., 2006. Pyrimidine and purine biosynthesis and degradation in plants. Annu. Rev. Plant Biol. 57, 805–836. https://doi.org/10.1146/annurev.arplant.57.032905.105421.